

Magnetic anisotropy reversal by shear stress in (110)-orientated La_{2/3}Ca_{1/3}MnO₃ films

Y. Li, J. R. Sun, J. Zhang, and B. G. Shen

Citation: *Journal of Applied Physics* **116**, 043916 (2014); doi: 10.1063/1.4891638

View online: <http://dx.doi.org/10.1063/1.4891638>

View Table of Contents: <http://scitation.aip.org/content/aip/journal/jap/116/4?ver=pdfcov>

Published by the [AIP Publishing](#)

Articles you may be interested in

[Exchange bias induced by the fully strained La_{2/3}Ca_{1/3}MnO₃ dead layers](#)

J. Appl. Phys. **115**, 17D701 (2014); 10.1063/1.4857935

[Effects of ferroelectric-poling-induced strain on magnetic and transport properties of La_{0.67}Ba_{0.33}MnO₃ thin films grown on \(111\)-oriented ferroelectric substrates](#)

Appl. Phys. Lett. **103**, 132910 (2013); 10.1063/1.4822269

[Tuning in-plane magnetic anisotropy in \(110\) La_{2/3}Ca_{1/3}MnO₃ films by anisotropic strain relaxation](#)

Appl. Phys. Lett. **92**, 012508 (2008); 10.1063/1.2828701

[Magnetic switching in epitaxial \(110\) La_{2/3}Ca_{1/3}MnO₃ films](#)

J. Appl. Phys. **99**, 08C503 (2006); 10.1063/1.2151833

[Thickness dependence of the magnetic anisotropy in La_{2/3}Ca_{1/3}MnO₃ thin films grown on LaAlO₃ substrates](#)

J. Appl. Phys. **93**, 8059 (2003); 10.1063/1.1556936

The advertisement features a dark blue background with a film strip graphic on the left side. The text is centered and reads: 'Not all AFMs are created equal' in orange, 'Asylum Research Cypher™ AFMs' in white, and 'There's no other AFM like Cypher' in orange. At the bottom, the website 'www.AsylumResearch.com/NoOtherAFMLikeIt' is listed in white, and the Oxford Instruments logo is in the bottom right corner, with the tagline 'The Business of Science®' below it.

Not all AFMs are created equal
Asylum Research Cypher™ AFMs
There's no other AFM like Cypher

www.AsylumResearch.com/NoOtherAFMLikeIt

OXFORD
INSTRUMENTS
The Business of Science®

Magnetic anisotropy reversal by shear stress in (110)-orientated $\text{La}_{2/3}\text{Ca}_{1/3}\text{MnO}_3$ films

Y. Li, J. R. Sun,^{a)} J. Zhang, and B. G. Shen

Beijing National Laboratory for Condensed Matter Physics and Institute of Physics, Chinese Academy of Sciences, Beijing 100190, China

(Received 21 May 2014; accepted 18 July 2014; published online 31 July 2014)

In-plane magnetic anisotropy has been studied for the (110)-orientated $\text{La}_{2/3}\text{Ca}_{1/3}\text{MnO}_3$ (LCMO) films grown on SrTiO_3 (STO) and LaAlO_3 (LAO) substrates. Deviation from orthorhombic symmetry is observed in these two series of films, particularly for the films grown above LAO, which suffer from a strong shear strain. A switch of the magnetic easy axis between the [001] and [1-10] axes is observed for the LCMO/LAO films as structure deformation varies, while the LCMO/STO films exhibit a [001] easy axis. An analytical analysis of the influence of magnetoelastic energy on magnetic anisotropy is performed, and the dominative role of shear strain is revealed. The present work indicates that the lattice distortion provides a feasible approach towards magnetic engineering, leading to abundant magnetic phenomena. © 2014 AIP Publishing LLC.

[<http://dx.doi.org/10.1063/1.4891638>]

I. INTRODUCTION

The abundant physical phenomena in rare-earth manganites ($\text{R}_{1-x}\text{A}_x\text{MnO}_3$) (R = trivalent rare-earth ion, A = divalent alkaline-earth ion) with perovskite structure has aroused extensive interest in recent years.¹⁻⁵ Due to coexisted spin-lattice and orbital-lattice coupling, epitaxially strained manganite films can behave differently from their bulk counterparts, demonstrating various emergent phenomena.⁶⁻¹² For example, through tuning orbital occupancy via lattice strains, the $\text{La}_{1-x}\text{Sr}_x\text{MnO}_3$ films can be driven from the ferromagnetic (FM) to antiferromagnetic (AFM) state. The charge and orbital ordering (COO) transition in the manganite films can also be affected by lattice strains, and isotropic and anisotropic lattice strains produce completely different effects: the former depresses whereas the latter supports the COO order.¹³ Lattice strains are also the most ordinary stimulus modifying magnetic anisotropy on demand of fundamental or applied researches. Through substrate-film lattice mismatch, the lattice strain in the film can be feasibly tuned. Isotropic strain in (001)-orientated film is the most typical epitaxial strain and also the one that has been most intensively studied. It was found that, for example, for the manganite films with a compressive and a tensile strain, magnetic moment will align in the direction perpendicular to the film plane and in film plane, respectively.¹⁴ In contrast, effects of anisotropic strain, which exist in (110)-orientated film, are less addressed. Compared with isotropic strains, the anisotropic strains are considerably complex since the two in-plane (IP) crystallographic directions, [001] and [1-10], are no longer equivalent, and shear strains will generally occur ($\epsilon_{xy} \neq 0$). This greatly complicates the crystal structure of the film. However, anisotropic strain has advantage over the isotropic one in a sense it leads to magnetic and transport anisotropy.¹⁵⁻¹⁹ For example,

the magnetic anisotropy becomes more pronounced in (110) films, such as $\text{La}_{1-x}\text{Ca}_x\text{MnO}_3$ ²⁰ and $\text{La}_{1-x}\text{Sr}_x\text{MnO}_3$.^{17,21} We found that despite intensive studies, there are still obvious controversies in reported works. For example, for the (110)- $\text{La}_{2/3}\text{Ca}_{1/3}\text{MnO}_3$ (LCMO) films, some authors found that the IP magnetic easy axis is [001] direction,²⁰ whereas others claimed a [1-10] easy axis.²² It is still not very clear how lattice strain affects the crystal structure of the film and how the deformed structure affects magnetic anisotropy. Here, we report a systematic study of the influence of crystal structure on magnetic anisotropy for the (110) $\text{La}_{2/3}\text{Ca}_{1/3}\text{MnO}_3$ films grown on different substrates. We found that either tensile or compressive strain imposed by substrate leads to a deviation of the film structure from orthogonal symmetry, yielding shear strain. We further found that the magnetic easy axis is very sensitive to structure deformation, switching between the [001] and [1-10] axes as structure varies. A quantitative analysis shows that the shear strain plays a dominative role in determining the magnetic anisotropy of the film.

II. EXPERIMENTS

Two series of LCMO films with the thicknesses between 5 nm and 160 nm were grown on (110)- LaAlO_3 (LAO) or (110)- SrTiO_3 (STO) substrates by pulsed laser deposition. During the deposition, the substrate temperature was kept at 720 °C and O_2 pressure was maintained at 50 Pa. After deposition, the film was *in-situ* annealed for 15 min and then cooled down to the room temperature in an atmosphere of 1 bar O_2 . Film surface was analyzed by atomic force microscope (AFM), and crystal structure was determined by x-ray diffraction performed on a Bruker diffractometer (D8 Discover) with $\text{Cu } K_{\alpha 1}$ radiation. θ - 2θ linear scanning spectra, ω -scan rocking curves (RCs) and reciprocal space maps (RSMs) of the films were collected. Magnetization was measured by a quantum designed Superconducting Quantum Interference Device magnetometer (SQUID).

^{a)}Author to whom correspondence should be addressed. Electronic mail: jrsun@iphy.ac.cn

III. RESULTS AND DISCUSSIONS

Fig. 1 shows the selected AFM images of the LCMO films. All films exhibit flat surface, with the root-mean-square roughness of several nanometers, although high surface energy exists in the peculiar (110) plane. The lattice constants of bulk LCMO, LAO, and STO are 3.863 Å, 3.788 Å, and 3.905 Å, respectively. For the (110)-oriented film, the main IP crystal axis is [001]/[1-10] and the out-of-plane (OP) axis is [110]. The stress is defined by $\delta = Y\varepsilon$, where Y is the Young modulus and ε is lattice strain. Y is determined by atomic arrangement and bond strengths, and is generally different along the [001] and [1-10] directions. The lattice mismatch is -1.9% between LCMO and LAO and 1.1% between LCMO and STO. Therefore, an IP anisotropic stress will be compressive in a coherently grown LCMO/LAO film and tensile in the LCMO/STO film. From the high resolution θ - 2θ scans (not shown), the OP lattice parameter, $d_{[110]}$, was found to relax gradually with increasing film thickness.

To determine the a , b , and c lattice parameters of the films, and the angle between two successive axes, the RSMs around two asymmetric reflections, (222)/(221) and (130), are collected, and depicted on the $q_{(1-10)}$ - $q_{(001)}$ plane. As shown in Fig. 2, the (222) or (221) reflection of the film has exactly the same q_{001} value as that of the STO, indicating a full strain in the film along the [001] axis. As indicated by the shift of the (130) peak, a gradual lattice relaxation occurs along the [1-10] axis for the films thicker than 45 nm. For the LCMO/LAO films, as shown by the RSMs of the (130) reflections in Fig. 3, lattice relaxation occurs along the [1-10] axis above 36 nm. Notably, the (222) reflections of the 36-nm-thick and 45-nm-thick LCMO/LAO films (Figs. 3(c) and 3(e)) show a c -axis lattice parameter much smaller than that of other LCMO/LAO films. Meanwhile, the (222) peak of the LAO substrate broadens towards high q_{001} values, indicating the presence of a low c phase, superimposed on normal LAO phase. The low c phase may mainly exist in the top layer of the substrate. Thus, the epitaxial grown LCMO film above this layer has a small c . This result indicates that the LAO substrate with a deformed top layer induces a more severely distorted structure in the films. Hereafter, these two films will be referred to as “special samples” whereas other films as “normal samples”.

Based on the RSMs of the (222) and (130) asymmetric reflections, the lattice constants and the angle between two successive axes of the unit cell can be determined. As shown in Figs. 4(a) and 4(d), the lattice constant relaxes slowly to bulk value at different rates along the [1-10] and [001] directions for both sets of films, except for the two special samples marked by a shadow area in Fig. 4(d). We define a quantity $R = (d_{\text{LCMO}}^{\text{film}} - d_{\text{substrate}}) / (d_{\text{LCMO}}^{\text{bulk}} - d_{\text{substrate}})$ to describe lattice relaxation, based on lattice constant d . The R -thickness relations in Figs. 4(b) and 4(e) show a more significant lattice relaxation along the [1-10] direction than along the [001] direction. This different elastic response is understandable noting the fact that the lattice strain in the [1-10] direction can be easily released through two flexible axes, a and b , whereas the c -axis is tightly clamped by the substrate. The deduced lattice parameters are shown in Figs. 4(c) and 4(f). With the decrease of film thickness, a , b , and c change slightly, whereas the angle γ between the a and b axes varies significantly from $\sim 90^\circ$ to $\sim 91.5^\circ$ for the LCMO/STO films and from $\sim 90^\circ$ to $\sim 87.5^\circ$ for the LCMO/LAO films. These results indicate a severe deviation from orthogonal structure of the (110) films and the occurrence of shear stress. As expected, the two special samples (shadowed area in Figs. 4(d)–4(f)) exhibit a structure deformation different from that of other films, with a less shear strain but a severer compressive strain.

The magnetization-magnetic field loops of the LCMO films, measured at 10 K along the [001] and [1-10] directions, respectively, were shown in Fig. 5. They show the typical features of uniaxial magnetic anisotropy. All films except for 36-nm-thick LCMO/STO film exhibit the typical FM behaviors. In contrast, the initial M - H curve of the 36-nm-thick LCMO/STO film undergoes a meta-magnetic transition above the field of 3 T (inset in Fig. 5(c)). It is possible that the FM and AFM phases coexist in this film, and the magnetic field yields an AFM-FM transition. A monotonic increase in saturation magnetization with film thickness is observed. However, the maximal value $\sim 3.06 \mu_B/\text{Mn}$ (obtained for the film of 160 nm) is still much lower than the expected value ($3.67 \mu_B/\text{Mn}$). Similar results have been obtained before, and were ascribed to the presence of an AFM layer in proximity of the interface.²² For the LCMO/STO films, [001] is magnetic easy axis, which is consistent with the results of other groups.²⁰ For the LCMO/LAO films, fascinatingly, the easy axis is the [1-10] axis for the two

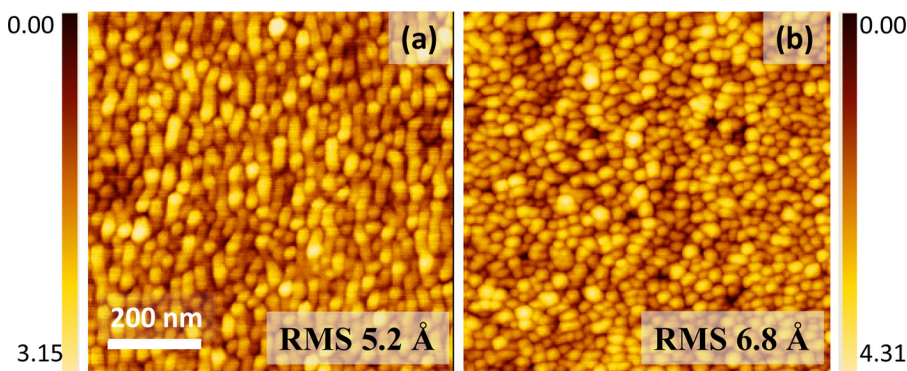


FIG. 1. AFM images of the (a) LCMO/STO and (b) LCMO/LAO films of 50 nm in thickness.

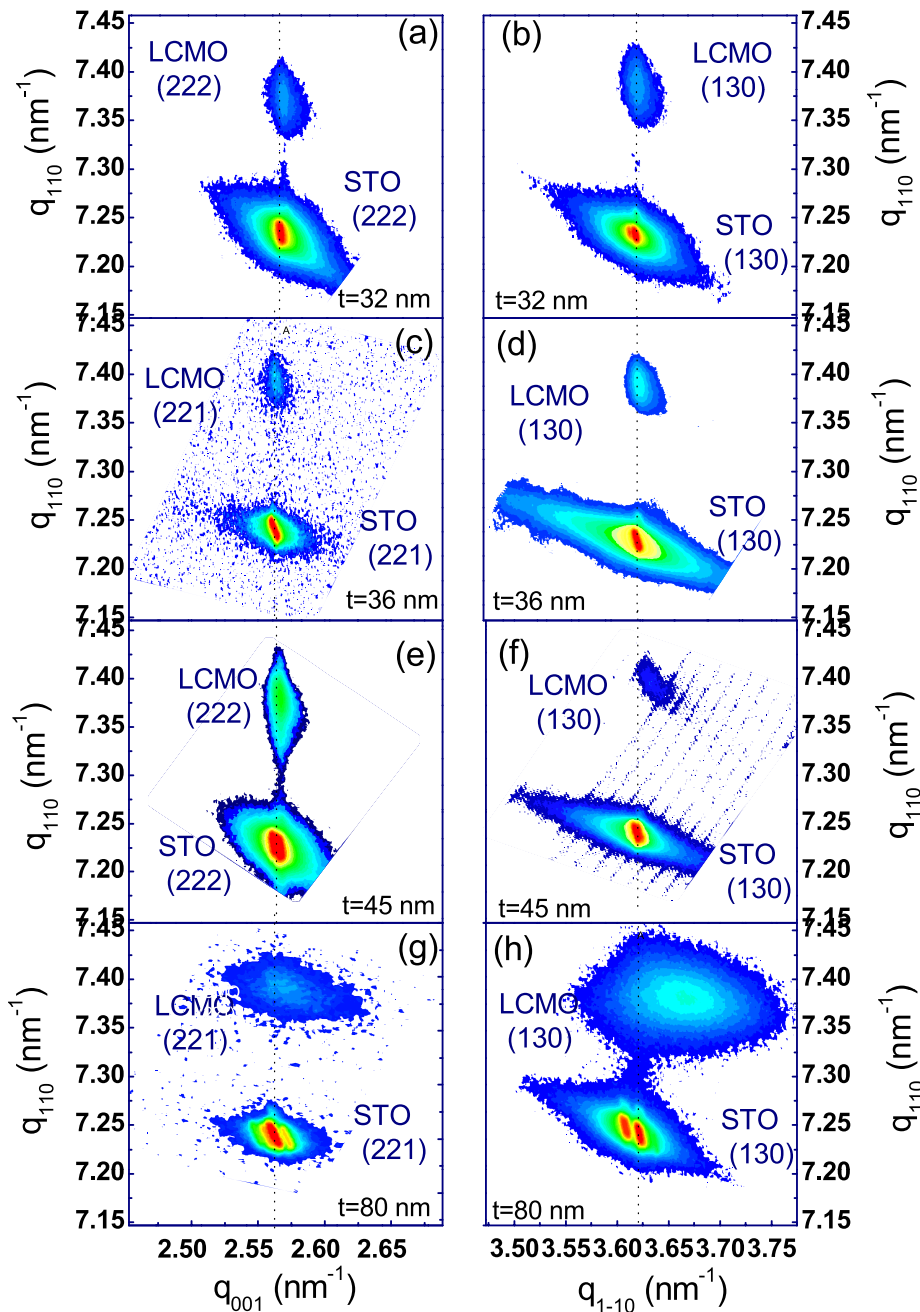


FIG. 2. RSMs of asymmetric reflections of the LCMO/STO films of different thicknesses. (a) 32 nm (222), (b) 32 nm (130), (c) 36 nm (221), (d) 36 nm (130), (e) 45 nm (222), (f) 45 nm (130), (g) 80 nm (221), and (h) 80 nm (130).

special samples, though the [001] axis is still the easy axis for other normal samples. This result indicates a structure deformation-induced a reversal of magnetic anisotropy axis. The magnetic anisotropy energy (MAE), defined by $\Delta E_{\text{MAE}} = E_{\text{MH}[1-10]} - E_{\text{MH}[001]}$, has been calculated from the M - H loops marked by grey shades (Fig. 5(f)) and shown in Fig. 7, which will be discussed below.

According to previous reports, IP uniaxial magnetic anisotropy can be induced by stepped surface or orientated domain structure.^{21,24,25} We excluded the presence of surface steps in our films (Fig. 1). Noting that the two special LCMO/LAO films (36 and 45 nm in thickness) with a distinct magnetic anisotropy own a distinctly deformed structure, the magnetic anisotropy should be strongly correlated with the lattice strains, i.e., the shear strain in films plays an important role in determining magnetic anisotropy.

For a magnetic system in a given strain state, the magnetostriction study reveals that MAE depends on not only the direction of \vec{M} (described by direction cosine α) but also the strain tensor elements ϵ (ϵ_{ij} is the component of strain tensor). Following Kittel²⁶ and Lee,²⁷ the magnetic-elastic anisotropy energy (MEE) can be decomposed into three parts, i.e., the first-order magnetocrystalline anisotropy energy $E_{\text{intrinsic}}$, that is expressed in terms of α , the magneto-elastic energy E_{mee} which is described by mixed α and ϵ terms, and the elastic energy E_{elas} that has only the ϵ terms.²⁸ Here, we use the room-temperature x-ray diffraction data to calculate strain tensor since the thermal expansion of LCMO, STO, and LAO are small and close to each other below 300 K.²⁹ For the LCMO films, the first-order magnetocrystalline anisotropy constant K_1 is reported to be $1 \times 10^4 \text{ erg/cm}^3$,³⁰ much smaller than the magneto-elastic energy, which is in the order of 10^6 erg/cm^3 as will be seen below. We therefore believed that the magnetic

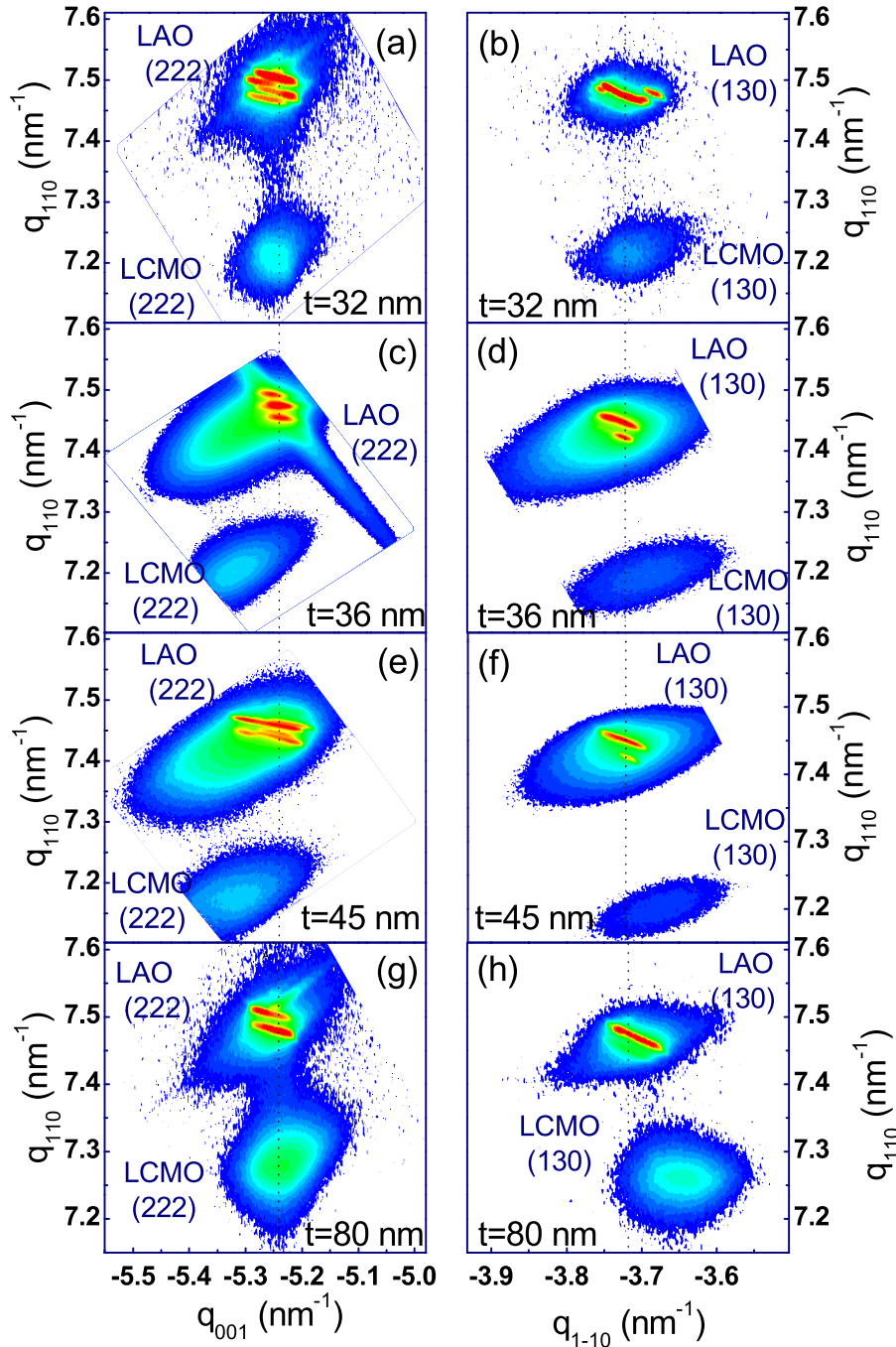


FIG. 3. RSMs of asymmetric reflections of the LCMO/LAO films of different thicknesses: (a) 32 nm (222), (b) 32 nm (130), (c) 36 nm (222), (d) 36 nm (130), (e) 45 nm (222), (f) 45 nm (130), (g) 80 nm (222), and (h) 80 nm (130).

anisotropy is dominated by magneto-elastic anisotropy, and simply ignored $E_{\text{intrinsic}}$ in the following derivations:^{17,20}

$$E = E_{\text{intrinsic}} + E_{\text{mee}} + E_{\text{elas}}, \quad (1)$$

$$E_{\text{intrinsic}} = K_1 \sum_{i>j} \alpha_i \alpha_j, \quad (2)$$

$$E_{\text{mee}} = b_1 \sum_i \alpha_i^2 \epsilon_{ii} + b_2 \sum_{i>j} \alpha_i \alpha_j \epsilon_{ij}, \quad (3)$$

$$E_{\text{elas}} = \frac{c_{11}}{2} \sum_i \epsilon_{ii}^2 + c_{12} \sum_{i>j} \epsilon_{ii} \epsilon_{jj} + \frac{c_{44}}{2} \sum_{i>j} \epsilon_{ij}^2, \quad (4)$$

where c_{ij} are the elastic constants, b_1 and b_2 are the magneto-elastic coupling coefficients, and can be expressed by the magnetostriction coefficients λ_{100} and λ_{111} by

$$b_1 = -3(c_{11} - c_{12})\lambda_{100}/2, \quad (5)$$

$$b_2 = -3c_{44}\lambda_{111}. \quad (6)$$

For pseudo-cubic structure, we can assume that λ is isotropic, i.e., $\lambda_{100} = \lambda_{111} = 5.5 \times 10^{-5}$.^{30,31} As shown in Fig. 6, the deviation from orthorhombic structure leads to shear strains, namely, $\epsilon_{xy} = \epsilon_{yx} \neq 0$. This deformation produces nondiagonal matrix elements. With the aid of Fig. 6, the elements of the strain tensor can be deduced, and described in Eqs. (7)–(11). It is worth noting that the two different types of IP strains, tensile stress in LCMO/STO and compressive stress in LCMO/LAO, give rise to different shear strain tensors

$$\epsilon_{xx} = (a \cos \beta - a_0)/a_0 \cong \cos \beta - 1, \quad (7)$$

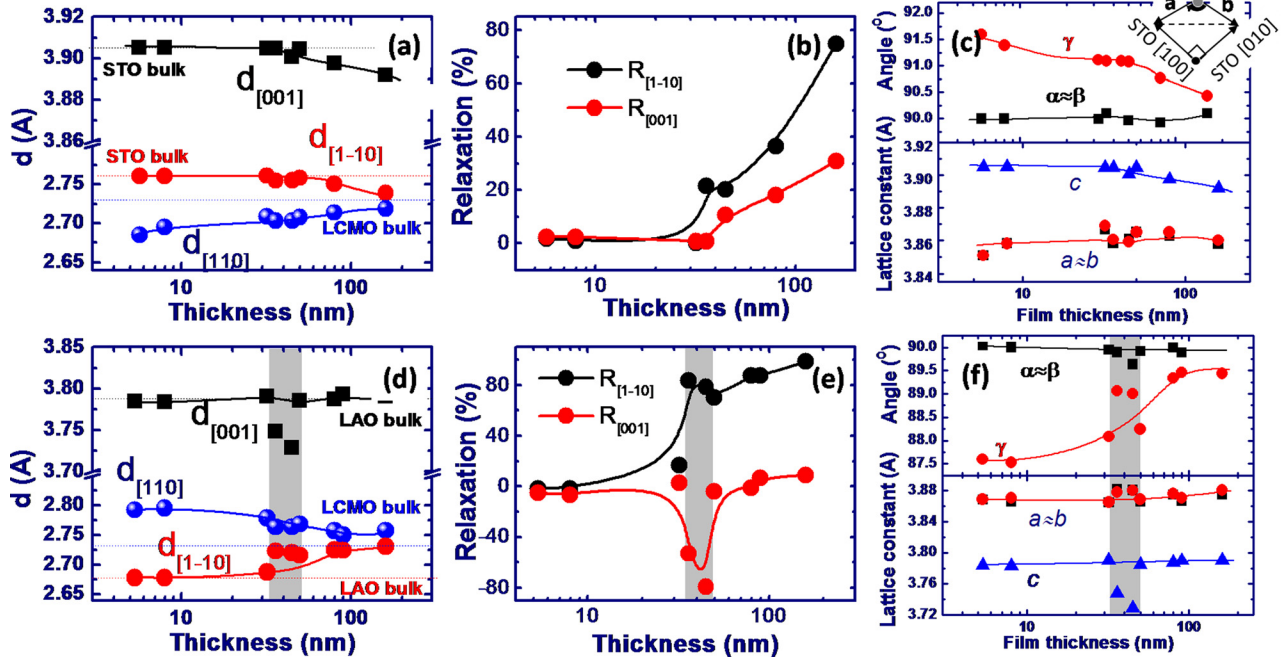


FIG. 4. Structure parameters and lattice relaxation as functions of film thickness. (a)–(c) the LCMO/STO films. (d)–(f) the LCMO/LAO films. Inset in (c) is a schematic diagram of lattice deformation. The shaded area represents the two special LCMO/LAO samples (36 and 45 nm).

$$\epsilon_{xx} = \epsilon_{yy}, \quad (8)$$

$$\epsilon_{zz} = \epsilon_{[001]}, \quad (9)$$

$$\epsilon_{xy} = [(a/a_0)\sin\beta + (c/c_0)\sin\beta]/2 \cong \sin\beta, \quad (10)$$

$$\beta = (\pi/2 - \gamma)/2. \quad (11)$$

In the following, we will show the analysis of the MEE for three special cases, for which the magnetization \vec{M} orients along three crystal axes [001], [1-10], and [110], respectively. At first, when $\vec{M} // [001]$, $\alpha_X = \alpha_Y = 0$, $\alpha_Z = 1$, we have

$$\begin{aligned} E_{[001]} &= E_{\text{intrinsic}} + E_{\text{mee}} + E_{\text{elas}} \\ &= (E_{\text{intrinsic}} + E_{\text{elas}}) + b_1 \sum_i \alpha_i^2 \epsilon_{ii} + b_2 \sum_{i>j} \alpha_i \alpha_j \epsilon_{ij} \\ &= (E_{\text{intrinsic}} + E_{\text{elas}}) + b_1 \epsilon_{zz} \\ &= (E_{\text{intrinsic}} + E_{\text{elas}}) - \frac{3}{2} (c_{11} - c_{12}) \lambda_{100} \epsilon_{zz}. \end{aligned} \quad (12)$$

Similarly,

$$\begin{aligned} E_{[1\bar{1}0]} &= (E_{\text{intrinsic}} + E_{\text{elas}}) - \frac{3}{2} (c_{11} - c_{12}) \lambda_{100} \epsilon_{xx} \\ &\quad + \frac{3}{2} c_{44} \lambda_{111} \epsilon_{xy}, \end{aligned} \quad (13)$$

$$\begin{aligned} E_{[110]} &= (E_{\text{intrinsic}} + E_{\text{elas}}) - \frac{3}{2} (c_{11} - c_{12}) \lambda_{100} \epsilon_{xx} \\ &\quad - \frac{3}{2} c_{44} \lambda_{111} \epsilon_{xy}. \end{aligned} \quad (14)$$

Which direction, [001] or [1-10], is easy direction is determined by which energy, E_{001} or $E_{1\bar{1}0}$, is lower. Adopting the parameters $c_{11} = 350$ GPa, $c_{12} = 113$ GPa, and $c_{44} = 150$ GPa for the LCMO films according to Refs. 20, 30 and 32, we have

$$\begin{aligned} \Delta E_{\text{MEE}} &= E_{[001]} - E_{[1\bar{1}0]} \\ &= -\frac{3}{2} \lambda [(c_{11} - c_{12})(\epsilon_{zz} - \epsilon_{xx}) + c_{44} \epsilon_{xy}]. \end{aligned} \quad (15)$$

Taking the 32-nm-thick LCMO/STO film as an example, we obtain the strain tensor matrix

$$\epsilon = \begin{pmatrix} \epsilon_{xx} & \epsilon_{xy} & 0 \\ \epsilon_{yx} & \epsilon_{yy} & 0 \\ 0 & 0 & \epsilon_{zz} \end{pmatrix} = \begin{pmatrix} -0.0047 & -0.967 & 0 \\ -0.967 & -0.0047 & 0 \\ 0 & 0 & 1.08 \end{pmatrix} \%. \quad (16)$$

From Eq. (15), we have $\Delta E_{\text{MEE}} = E_{[001]} - E_{[1\bar{1}0]} = -9.2409 \times 10^5$ ergs/cm³. This value is almost equal to ΔE_{MAE} , deduced from integration of the M - H curves ($\Delta E_{\text{MAE}} = E_{\text{MH}[1-10]} - E_{\text{MH}[001]} = -7.428 \times 10^5$ ergs/cm³), which indicates that the easy axis is along the [001] direction.

Second, for the 32-nm-thick LCMO/LAO film, which is in the normal stress state, the strain tensor matrix is

$$\epsilon = \begin{pmatrix} \epsilon_{xx} & \epsilon_{xy} & 0 \\ \epsilon_{yx} & \epsilon_{yy} & 0 \\ 0 & 0 & \epsilon_{zz} \end{pmatrix} = \begin{pmatrix} -0.014 & 1.67 & 0 \\ 1.67 & -0.014 & 0 \\ 0 & 0 & -1.88 \end{pmatrix} \%. \quad (17)$$

Thus, we get $\Delta E_{\text{MEE}} = E_{[001]} - E_{[1\bar{1}0]} = -4.954 \times 10^5$ ergs/cm³. This value is in good agreement with ΔE_{MAE} , $\Delta E_{\text{MAE}} = E_{\text{MH}[1-10]} - E_{\text{MH}[001]} = -7.542 \times 10^5$ ergs/cm³, indicating that the easy axis is [001].²³

Third, for the special sample, 36-nm-thick LCMO/LAO film, we found that the distinct structure deformation yields a much larger ϵ_{zz}

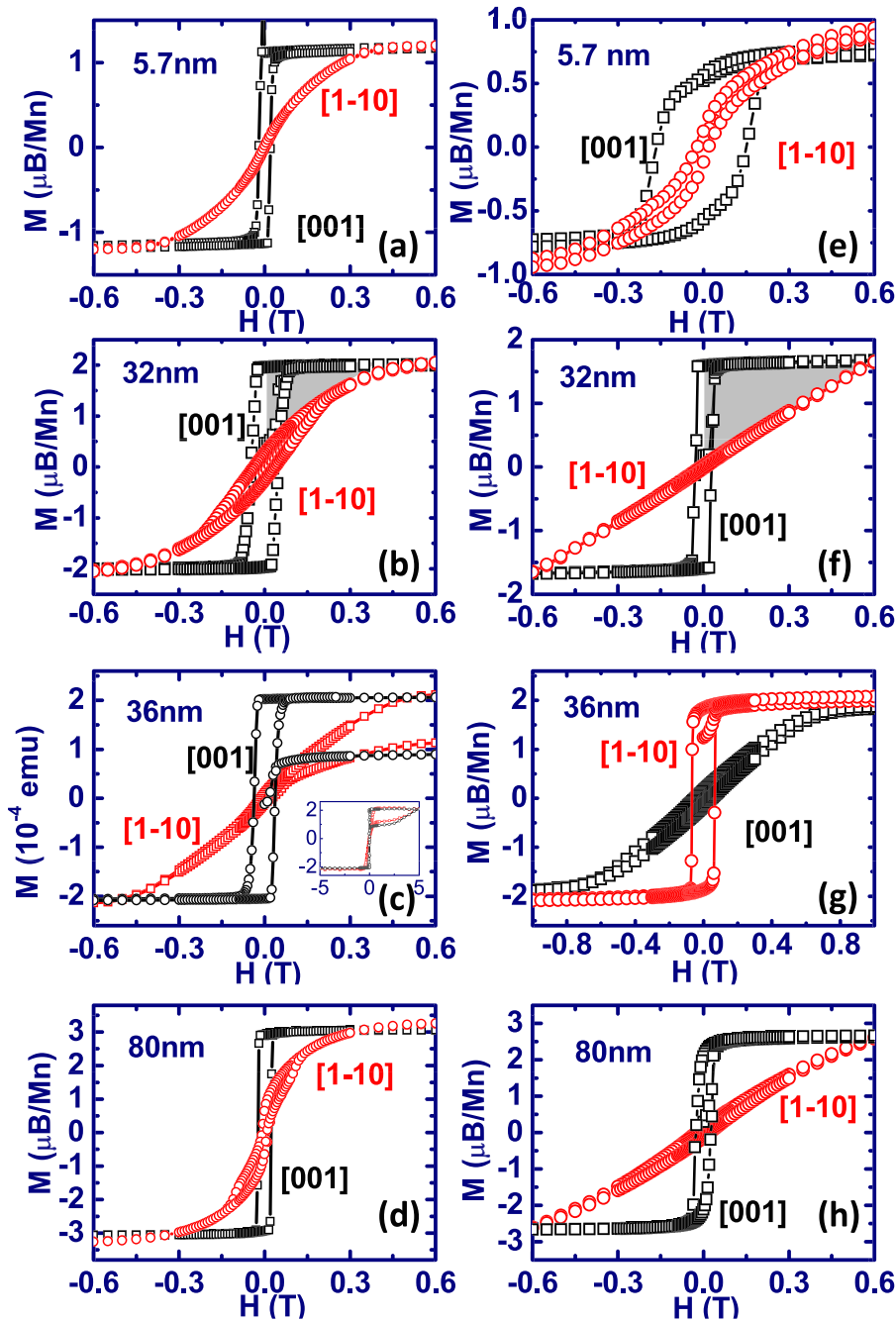


FIG. 5. Magnetization-magnetic field loops of the LCMO/STO films ((a)–(d)) and the LCMO/LAO films ((e)–(h)), measured at 10K with the magnetic field applied along the [001] and the [1–10] directions, respectively. Inset in 5(c) is the complete M - H curve of the 36 nm LCMO/STO film.

$$\epsilon = \begin{pmatrix} \epsilon_{xx} & \epsilon_{xy} & 0 \\ \epsilon_{yx} & \epsilon_{yy} & 0 \\ 0 & 0 & \epsilon_{zz} \end{pmatrix} = \begin{pmatrix} -0.00335 & 0.819 & 0 \\ 0.819 & -0.00335 & 0 \\ 0 & 0 & -2.97 \end{pmatrix} \% \quad (18)$$

The calculated $\Delta E_{MEE} = E_{[001]} - E_{[1\bar{1}0]} = 1.028 \times 10^5 \text{ ergs/cm}^3$, while the ΔE_{MAE} is $\sim 1.134 \times 10^6 \text{ ergs/cm}^3$. Positive ΔE_{MAE} implies a magnetic reversal of the easy axis from the [001] to the [1-10] axis. The agreement of ΔE_{MAE} and ΔE_{MEE} indicates the latter is the reason for the magnetic reversal. In fact, for the LCMO/STO films, $|\epsilon_{xx}| \ll |\epsilon_{zz}|$,

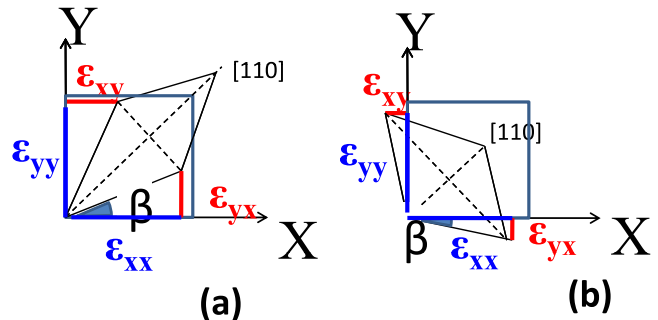


FIG. 6. A schematic for the derivation of strain tensor of (a) LCMO/LAO and (b) LCMO/STO. ϵ_{xx} , ϵ_{yy} , and ϵ_{zz} are linear strains, and ϵ_{xy} , ϵ_{yx} are shear strains.

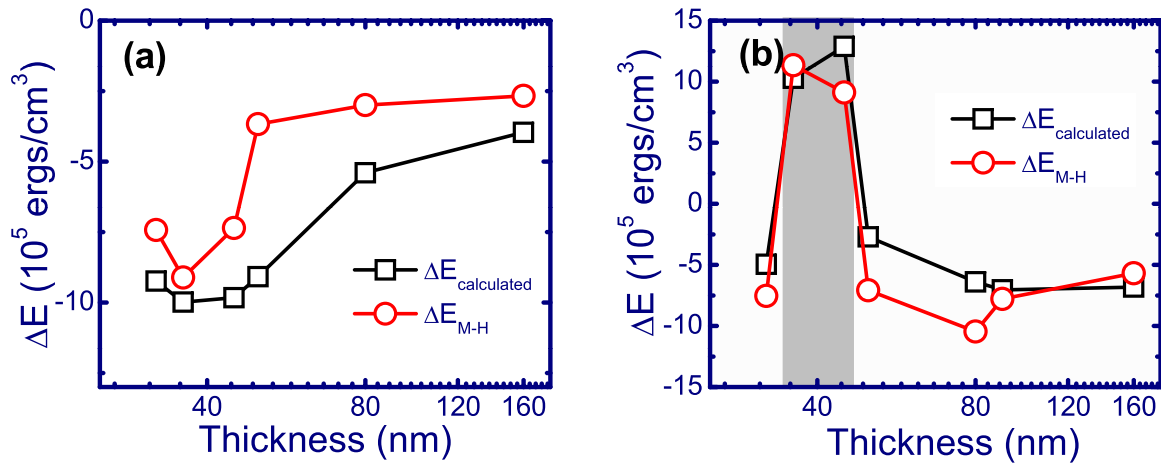


FIG. 7. Thickness dependence of the magnetic anisotropy energy for the (a) LCMO/STO and (b) LCMO/LAO films. ΔE_{MAE} and ΔE_{MEE} are calculated by integrating in M - H curves and Eq. (15), respectively.

$$\begin{aligned}\Delta E_{MEE} &= E_{[001]} - E_{[1\bar{1}0]} \\ &= -\frac{3}{2}\lambda[(c_{11} - c_{12})(\epsilon_{zz} - \epsilon_{xx}) + c_{44}\epsilon_{xy}] \\ &\approx -\frac{3}{2}\lambda[(c_{11} - c_{12})\epsilon_{zz} + c_{44}\epsilon_{xy}].\end{aligned}\quad (19)$$

According to the above equation, we can predict that it is possible for LCMO/STO films to favor the $[1-10]$ easy axis, as has been observed by Guo.²²

In Fig. 7 we show all calculated ΔE_{MEE} . The correspondence of the ΔE_{MAE} and the ΔE_{MEE} reveals the dominative role of the former in determining the magnetic easy axis of the films. The analytical analysis reveals the importance of shear stress for the controlling of magnetic anisotropy clarifying the controversies in previous reports. We ascribe the minor discrepancy between these two types of energies to calculation error.

IV. SUMMARY

We have carried out a systemic study on the correlation between crystal structure and magnetic anisotropy for (110) LCMO films grown on the STO and LAO substrates. We found that either tensile or compressive strains imposed by substrates lead to a deviation of the crystal structure from orthogonal symmetry, and the magnetic easy axis is very sensitive to the details of the structure deformation. A magnetic reversal of the easy axis from the $[001]$ to $[1-10]$ axis is observed for the LCMO/LAO films with different shear strains. In contrast, the LCMO/STO films maintain an $[001]$ easy axis. An analytical analysis of the magnetic anisotropy energy and magneto-elastic energy is performed, special attention was paid to the effect of shear strains. Based on this analysis, we interpreted the magnetic reversal and clarified the controversies in previous reports. The present work reveals that lattice distortion can be utilized to generate abundant magnetic phenomena, proving a feasible approach towards magnetic engineering.

ACKNOWLEDGMENTS

This work has been supported by the National Basic Research of China, the National Natural Science Foundation

of China, the Knowledge Innovation Project of the Chinese Academy of Science, the Beijing Municipal Nature Science Foundation.

- ¹S. Jin, T. H. Tiefel, M. McCormack, R. A. Fastnacht, R. Ramesh, and L. H. Chen, *Science* **264**, 413 (1994).
- ²E. Dagotto, T. Hotta, and A. Moreo, *Phys. Rep.* **344**, 1 (2001).
- ³J. C. Loudon, N. D. Mathur, and P. A. Midgley, *Nature* **420**, 797 (2002).
- ⁴D. Kim, B. L. Zink, F. Hellman, and J. M. D. Coey, *Phys. Rev. B* **65**, 214424 (2002).
- ⁵Q. Huang, A. Santoro, J. W. Lynn, R. W. Erwin, J. A. Borchers, J. L. Peng, K. Ghosh, and R. L. Greene, *Phys. Rev. B* **58**, 2684 (1998).
- ⁶J. M. D. Coey, M. Viret, and S. Von Molnar, *Adv. Phys.* **48**, 167 (1999).
- ⁷H. S. Wang, Q. Li, K. Liu, and C. L. Chien, *Appl. Phys. Lett.* **74**, 2212 (1999).
- ⁸A. Biswas, M. Rajeswari, R. C. Srivastava, T. Venkatesan, R. L. Greene, Q. Lu, A. L. de Lozanne, and A. J. Millis, *Phys. Rev. B* **63**, 184424 (2001).
- ⁹K. J. Lai, M. Nakamura, W. Kundhikanjana, M. Kawasaki, Y. Tokura, M. A. Kelly, and Z. X. Shen, *Science* **329**, 190 (2010).
- ¹⁰W. Prellier, M. Rajeswari, T. Venkatesan, and R. L. Greene, *Appl. Phys. Lett.* **75**, 1446 (1999).
- ¹¹C. Kwon, M. C. Robson, K. C. Kim, J. Y. Gu, S. E. Lofland, S. M. Bhagat, Z. Trajanovic, M. Rajeswari, T. Venkatesan, A. R. Kratz, R. D. Gomez, and R. Ramesh, *J. Magn. Magn. Mater.* **172**, 229 (1997).
- ¹²A. M. Haghiri-Gosnet, J. Wolfman, B. Mercey, C. Simon, P. Lecoeur, M. Korzenki, M. Hervieu, R. Desfeux, and G. Baldinozzi, *J. Appl. Phys.* **88**, 4257 (2000).
- ¹³M. Nakamura, Y. Ogimoto, H. Tamaru, M. Izumi, and K. Miyano, *Appl. Phys. Lett.* **86**, 182504 (2005).
- ¹⁴J. Dho, Y. N. Kim, Y. S. Hwang, J. C. Kim, and N. H. Hur, *Appl. Phys. Lett.* **82**, 1434 (2003).
- ¹⁵Y. Suzuki, H. Y. Hwang, S. W. Cheong, and R. B. van Dover, *Appl. Phys. Lett.* **71**, 140 (1997).
- ¹⁶M. Bibes, V. Laukhin, S. Valencia, B. Martinez, J. Fontcuberta, O. Y. Gorbenko, A. R. Kaul, and J. L. Martinez, *J. Phys.: Condens. Matter* **17**, 2733 (2005).
- ¹⁷L. M. Berndt, V. Balbarin, and Y. Suzuki, *Appl. Phys. Lett.* **77**, 2903 (2000).
- ¹⁸I. C. Infante, F. Sanchez, J. Fontcuberta, M. Wojcik, E. Jedryka, S. Estrade, F. Peiro, J. Arbiol, V. Laukhin, and J. P. Espinos, *Phys. Rev. B* **76**, 224415 (2007).
- ¹⁹H. Boschker, M. Mathews, E. P. Houwman, H. Nishikawa, A. Vailionis, G. Koster, G. Rijnders, and D. H. A. Blank, *Phys. Rev. B* **79**, 214425 (2009).
- ²⁰I. C. Infante, J. O. Osso, F. Sanchez, and J. Fontcuberta, *Appl. Phys. Lett.* **92**, 012508 (2008).
- ²¹P. Perna, C. Rodrigo, E. Jimenez, F. J. Teran, N. Mikuszeit, L. Mikuszeit, L. Mechin, J. Camarero, and R. Miranda, *J. Appl. Phys.* **110**, 013919 (2011).

- ²²N. L. Guo, J. Li, Y. F. Wei, Y. Zhang, L. M. Cui, L. Zhao, Y. R. Jin *et al.*, *J. Appl. Phys.* **112**, 013907 (2012).
- ²³H. Boschker, J. Kautz, E. P. Houwman, G. Koster, D. H. A. Blank, and G. Rijnders, *J. Appl. Phys.* **108**, 103906 (2010).
- ²⁴M. Mathews, F. M. Postma, J. C. Lodder, R. Jansen, G. Rijnders, and D. H. A. Blank, *Appl. Phys. Lett.* **87**, 242507 (2005).
- ²⁵Z. H. Wang, G. Cristiani, and H. U. Habermeier, *Appl. Phys. Lett.* **82**(21), 3731 (2003).
- ²⁶C. Kittel, *Rev. Mod. Phys.* **21**, 541 (1949).
- ²⁷E. W. Lee, *Rep. Prog. Phys.* **18**, 184 (1955).
- ²⁸D. Sander, *Rep. Prog. Phys.* **62**, 809 (1999).
- ²⁹The linear thermal expansion coefficients is $\sim 1.12 \times 10^{-5}/\text{K}$ in the temperature range 50–1000 °C for LCMO [M. Mori, Y. Hiei, N. M. Sammes, and G. A. Tompsett, *J. Electrochem. Soc.* **147**, 1295 (2000)], and $2.59 \times 10^{-5}/\text{K}$ in the temperature range 110–300 K for STO [K. Itoh, K. Ochiai, H. Kawaguchi, C. Moriyoshi, and E. Nakamura, *Ferroelectrics* **159**, 85 (1994)]. Thus, the relative changes of lattice constants can be estimated, and they are $\sim 0.38\%$ and $\sim 0.86\%$ from room temperature down to 10 K for LCMO and STO, respectively. The thermal volume expansion of LAO is also small as shown by B. C. Chakoumakos, D. G. Schlom, M. Urbanik, and J. Luine, *J. Appl. Phys.* **83**, 1979 (1998).
- ³⁰M. Ziese, H. C. Semmelhack, and P. Busch, *J. Magn. Magn. Mater.* **246**, 327 (2002).
- ³¹S. Chikazumi, *Physics of Ferromagnetism* (Clarendon Press, Oxford, 1997).
- ³²J. H. So, J. R. Gladden, Y. F. Hu, J. D. Maynard, and Q. Li, *Phys. Rev. Lett.* **90**, 036103 (2003).